First-principles calculation of *ortho–para* effects in the second virial coefficients of H_2 and D_2 at low temperatures

Giovanni Garberoglio*,† and Allan H. Harvey*,‡

†European Centre for Theoretical Studies in Nuclear Physics and Related Areas (FBK-ECT), Trento, I-38123, Italy.*

‡Applied Chemicals and Materials Division, National Institute of Standards and Technology, Boulder, CO 80305, USA.

E-mail: garberoglio@ectstar.eu; allan.harvey@nist.gov

Abstract

We report *ab initio* calculations of the second virial coefficient $B(T)$ of molecular hydrogen isotopologues in the rigid-rotor approximation using the path-integral Monte Carlo method. We present a novel method for efficient sampling of rotational degrees of freedom based on Doob's h-transform that can be used with any spin isomer, including those for which the quantum mechanical propagator in imaginary time is negative, e.g. *ortho*-H_2. Additionally, we extend the theory to evaluate the contribution to $B(T)$ due to quantum statistical effects, relevant at low temperatures. This allows us to compute the difference in $B(T)$ between *para*-H_2 and normal H_2; our calculation of this difference near 20 K is in qualitative agreement with the only available experimental measurements.

Introduction

Hydrogen (H_2) has long been of interest in many industrial and scientific contexts. Industrial uses include metallurgy, ammonia production, petroleum refining, fuel cells, and rocketry, while scientific interests include planetary science and temperature metrology. Recently, there has been growing interest in hydrogen as an energy carrier. The thermophysical properties of hydrogen are essential to design of liquefaction processes and for transportation of hydrogen.[1]

Molecular hydrogen has attracted much theoretical interest, because with only two electrons it is amenable to *ab initio* calculations of its properties whose accuracy can rival or even exceed that of the best experiments. Examples include single-molecule calculations of rovibrational energy levels[2] and polarizabilities,[3,4] and surfaces for the intermolecular potential between two hydrogen molecules.[5]

Calculating properties of H_2 from molecular physics, particularly those that are averages over a distribution of states, is complicated by the existence of spin isomers. Because of symmetry requirements on the wavefunction under exchange of identical nuclei, a homonuclear

diatomic molecule has constraints on its rotational states, affecting their statistical weight depending on whether the rotational quantum number J is even or odd. Interconversion between odd and even values of J is very slow (especially at cryogenic temperatures) unless a catalyst is present, so samples of hydrogen may be studied in which the population of states is not at thermodynamic equilibrium. As a result, one can delineate several different "flavors" of hydrogen.

In *para*-hydrogen (p-H_2), the spins of the hydrogen nuclei are in an antisymmetric state. For the H_2 molecule, because the nuclei are fermions, the molecule can only occupy rotational states with even values of J, including the rotational ground state which is $J = 0$. Because the deuterium nucleus is a boson, *para*-D_2 consists of molecules with odd J, beginning with $J = 1$. In *ortho*-hydrogen (o-H_2), the nuclear spins are in a symmetric state. This restricts the rotational states to odd J for the H_2 molecule and even J (including the rotational ground state $J = 0$) for D_2.

One can also consider *equilibrium* hydrogen (e-H_2), in which the rotational levels are occupied according to a Boltzmann distribution regardless of spin states; this can be achieved with the use of a catalyst. The equilibrium *ortho*/*para* proportion varies with temperature; in the low-temperature limit all molecules have $J = 0$ so that e-H_2 is 100% p-H_2 while e-D_2 is 100% o-D_2. At high temperatures, the outcome of the statistics is that e-H_2 is 3/4 o-H_2 and 1/4 p-H_2, while e-D_2 becomes 2/3 o-D_2 and 1/3 p-D_2.

Finally, many scientific studies have used *normal* hydrogen (n-H_2), which is the high-temperature limiting composition defined in the preceding paragraph. Because of slow interconversion, it is possible to prepare n-H_2 or n-D_2 at a high temperature and then study it at cryogenic temperatures.

In this work, we study the effect of spin isomers on the second virial coefficient $B(T)$, which measures the initial (low-density) deviation of a fluid's thermodynamic behavior from that of an ideal gas. $B(T)$ is a function of the interaction between two molecules, and it differs among the different types of hydrogen because the intermolecular forces depend

(weakly) on the rotational states J. Different $B(T)$ functions exist for *para–para*, *ortho–ortho*, and *ortho–para* interactions. $B(T)$ for e-H_2 or n-H_2 can be calculated from these interactions in the same way $B(T)$ is calculated for a binary mixture.

Early attempts to measure the difference in $B(T)$ between p-H_2 and n-H_2 were inconclusive, but landmark results were achieved by Beenakker et al. in 1960.[6] They found a difference that was small but clearly nonzero, on the order of 2 cm^3/mol, at 20.5 K and at 18.3 K, with B for n-H_2 more negative. They were unable to measure any difference between o-D_2 and n-D_2 at 20.5 K.

In principle, there are two effects that could cause this difference. There is a purely quantum-statistical effect, where exchange effects differ between symmetric and antisymmetric states at low temperatures. This effect on $B(T)$ has been studied[7,8] and found to be tiny near 20 K, much too small (and in the wrong direction) to explain the difference observed by Beenakker et al.[6]

A qualitatively correct explanation for the observed difference was presented in 1961 by Knaap and Beenakker.[9] At low temperatures, essentially all p-H_2 molecules are in the $J = 0$ state, while all o-H_2 molecules are in the $J = 1$ state. Because of centrifugal stretching associated with rotation, the $J = 1$ state is elongated compared to the $J = 0$ state. This causes the electron distribution to be more spread out, giving the molecule a slightly larger polarizability. The larger polarizability produces a more negative potential energy between the molecules, making $B(T)$ more negative. The increased polarizability (and therefore larger attractive interactions) of rotationally stretched states has since been confirmed by high-accuracy quantum calculations of the polarizability of different rovibrational states.[3]

These differences have consequences for processes such as hydrogen liquefaction where it is desired to understand and control the populations of spin isomers. Because of the relative ease with which the H_2 molecule and its pair interactions can be described by theory, it is desirable to use theory to describe this effect. This is harder than it might seem, because no previous work has rigorously addressed *ortho–ortho* interactions for H_2.

In this work, we develop a rigorous approach to calculating $B(T)$ for homonuclear diatomic molecules in odd spin states (o-H_2, p-D_2). We supply the information needed to compute $B(T)$ for H_2 and D_2 in any mixture of spin states, and assess our ability to predict the difference between p-H_2 and n-H_2 measured by Beenakker et al.[6]

Previous computational efforts

To be concise, we will not review attempts to model hydrogen with simple, spherically symmetric forms such as the Lennard–Jones potential. We focus on efforts that use state-of-the-art *ab initio* methods to develop the pair potential, and that also account for quantum effects (which cannot be ignored due to the low mass and moment of inertia) in the calculation of $B(T)$.

Diep and Johnson[10] performed calculations at the CCSD(T) level and developed an anisotropic pair potential. They simplified this to an isotropic form, and used a path-integral Monte Carlo (PIMC) method on that simplified potential to account for translational quantum effects on $B(T)$. Harvey and Hodges[11] showed that the effect of ignoring anisotropy was not insignificant, and that the Diep–Johnson potential gave $B(T)$ in modest disagreement with experiment.

Patkowski et al.[5] developed a pair potential at a more complete quantum level; the molecules were considered rigid with a bondlength equal to its expectation value for the rovibrational ground state of H_2. $B(T)$ was computed with a PIMC method that fully accounted for quantum effects in both translation and rotation. The agreement with experiment was much improved over the Diep–Johnson results.

These results still contained an uncontrolled approximation; they treated the molecules as rigid rotors. In reality, the H_2 molecule is flexible, with rotational stretching producing greater average bondlengths with increasing temperature and all states sampling a distribution of bondlengths. A six-dimensional potential, incorporating the effect of different bondlengths, was developed at a moderately accurate quantum level by Hinde.[12] Gar-

beroglio et al.[13] developed what should be a more accurate six-dimensional potential by superimposing Hinde's flexibility correction on the high-quality four-dimensional rigid-rotor potential of Patkowski et al.[5] This potential was then evaluated at the expectation value of the bondlength at each temperature (for H_2, D_2, and HD) to produce an effective four-dimensional potential from which B was calculated by PIMC. The improvement for H_2 was small, but the approach allowed the first high-quality calculations of $B(T)$ for D_2 and HD, both of which were in fairly good agreement with experiment.

Rigorous use of a six-dimensional potential requires considering the flexibility throughout the calculations rather than making an effective four-dimensional potential and subsequently ignoring flexibility. This was accomplished by Garberoglio et al.,[14] who developed a PIMC approach that sampled the intramolecular flexibility in addition to the intermolecular degrees of freedom. It was found that the effect of flexibility on $B(T)$ was not negligible, especially at higher temperatures, although the overall agreement with experimental data was similar to previous work.

All of the PIMC work described in this section had a significant limitation; it was restricted to molecules with even J. In other words, it was only for p-H_2 or o-D_2, and its validity for other spin states is unclear. Those calculations were therefore inherently unable to address the difference between p-H_2 and n-H_2. The main reason for this limitation was the fact that the path-integral approach applied to o-H_2 or p-D_2 results in "probability distributions" with negative sign, which severely limits the use of Monte Carlo techniques. In this paper, we will review a solution for this problem, and present a new numerical technique that enables efficient sampling for these cases.

Methods

The second virial coefficient of rigid rotors

The second virial coefficient $B(T)$ at temperature T is given by[15,16]

$$B(T) = -\frac{Z_2(T) - Z_1^2(T)}{2V}, \tag{1}$$

where V is the volume of the system (with the limit $V \to \infty$ taken at the end of the calculations), and one defines

$$\frac{Z_N(T)}{N!} = \frac{Q_N(T)V^N}{Q_1^N(T)}, \tag{2}$$

where Q_N is the partition function of N molecules. In the following, we will be mainly interested in rigid-rotor models of identical diatomic molecules of mass m and moment of inertia I, hence we can write

$$Q_1(T) = n\frac{V}{\Lambda^3}q_{\rm rot}(T) \tag{3}$$

$$Q_2(T) = \frac{n^2}{2!}\sum_{\mathcal{P}} \mathrm{tr}\left(\mathrm{e}^{-\beta H}\mathcal{P}\right), \tag{4}$$

where $\beta = (k_{\rm B}T)^{-1}$, $k_{\rm B}$ is the Boltzmann constant, $\Lambda = h/\sqrt{2m\pi k_{\rm B}T}$ is the de Broglie thermal wavelength of a molecule of mass m, h is the Planck constant, $q_{\rm rot}$ is the partition function of the rotational degrees of freedom, and n is the number of degrees of freedom that do not explicitly enter in the two-body Hamiltonian H; in our case, n counts the nuclear spin states of each molecule. The Hamiltonian can be further written as $H = T_1 + T_2 + K_1 + K_2 + U_2$, where $T_i = -\hbar^2\nabla_i^2/(2m)$ is the translational kinetic energy operator of molecule i with mass m, $K_i = \hat{\mathbf{J}}_i^2/(2I)$ is the rotational kinetic energy operator of the linear molecule i with angular momentum $\hat{\mathbf{J}}_i$ and moment of inertia I, and $U_2(\mathbf{r};\boldsymbol{\Omega},\boldsymbol{\Omega}')$ denotes the interaction potential between two rigid rotors whose centers of mass are separated by $\mathbf{r}$ and are oriented along the directions $\boldsymbol{\Omega}$ and $\boldsymbol{\Omega}'$, respectively. The sum over $\mathcal{P}$ runs over the identity operator $\mathbf{1}$ and the

operator $\mathcal{E}$ that exchanges the coordinates of two molecules, including a positive sign in the case of bosons and a negative sign in the case of fermions, and the trace is performed on the relevant eigenstates of H (see the discussion below in the case of homonuclear molecules). Putting everything together, one can write:

$$B(T) = -\frac{1}{2V}\left[\frac{\Lambda^6}{q_{\mathrm{rot}}^2}\sum_{ij}\left(\langle ij|\mathrm{e}^{-\beta H}|ij\rangle \pm \frac{1}{n}\langle ij|\mathrm{e}^{-\beta H}|ji\rangle\right) - V^2\right], \tag{5}$$

where we have denoted by $|i\rangle$ a complete set of single-molecule states and performed the sum on the degrees of freedom that do not explicitly appear in H. The first term in the sum, which corresponds to considering distinguishable particles (Boltzmann statistics), is the primary contribution. The second term, which takes into account the quantum statistical properties of the molecules, is called the exchange term and is relevant only at low temperatures.[17] In the case of molecular hydrogen isotopologues, the choice of sign in Eq. (5) depends on the bosonic (+) or fermionic (−) nature of the interacting molecules, which is in turn determined by the total nuclear spin S: molecules with even S (e.g., p-H_2, o-H_2, o-D_2, p-D_2) are bosons, and molecules with odd S (e.g., HD) are fermions, hence the ± sign could be written as $(-1)^S$.

The path-integral formulation

Equation (5) is most usefully evaluated using the path-integral approach,[5,10,13,18] which uses the Trotter–Suzuki identity to write

$$\mathrm{e}^{-\beta H} = \lim_{P\to\infty}\left(\mathrm{e}^{-\beta T_1/P}\mathrm{e}^{-\beta T_2/P}\mathrm{e}^{-\beta K_1/P}\mathrm{e}^{-\beta K_2/P}\mathrm{e}^{-\beta U_2/P}\right)^P, \tag{6}$$

using a finite, but sufficiently large, value for P. Single-molecule states for both molecules are conveniently written in the coordinate representation, that is $|ij\rangle = |\mathbf{r}_1, \boldsymbol{\Omega}_1; \mathbf{r}_1', \boldsymbol{\Omega}_1'\rangle = |\mathbf{r}_1\rangle|\boldsymbol{\Omega}_1\rangle|\mathbf{r}_1'\rangle|\boldsymbol{\Omega}_1'\rangle$ where $|\mathbf{r}_1\rangle$ are the position eigenstates and $|\boldsymbol{\Omega}_1\rangle$ the direction eigenstates of one molecule, while the primed quantities correspond to the second molecule. A subscript

1 has been introduced for later convenience. Notice that the sum over i and j in Eq. (5) becomes, in the coordinate representation, an integral over the center-of-mass position and the orientation of both molecules. One is then left to evaluate, for each of the two linear rotors, matrix elements of the form $\langle \mathbf{r}_2|\mathrm{e}^{-\beta T_i/P}|\mathbf{r}_1\rangle$ and $\langle \mathbf{\Omega}_2|\mathrm{e}^{-\beta K_i/P}|\mathbf{\Omega}_1\rangle$. The matrix elements involving the translational coordinates can be evaluated analytically,[19] resulting in

$$\langle \mathbf{r}_2|\mathrm{e}^{-\beta T_i/P}|\mathbf{r}_1\rangle \equiv f(\mathbf{r}_2,\mathbf{r}_1;\Lambda^2/P) = \frac{P^{3/2}}{\Lambda^3}\exp\left(-\frac{\pi P}{\Lambda^2}\left|\mathbf{r}_2-\mathbf{r}_1\right|^2\right), \tag{7}$$

that is, a Gaussian function with variance $\Lambda^2/(2\pi P) = \hbar^2/(mk_{\mathrm{B}}TP)$. The matrix element involving the rotational coordinates can be written as[20]

$$\langle \mathbf{\Omega}_2|\mathrm{e}^{-\beta K_i/P}|\mathbf{\Omega}_1\rangle \equiv \varphi(\mathbf{\Omega}_2\cdot\mathbf{\Omega}_1;TP) = {\sum_{J=0}^{\infty}}' \frac{2J+1}{4\pi}\exp\left(-\frac{\beta J(J+1)\mathcal{B}}{P}\right)P_J(\mathbf{\Omega}_2\cdot\mathbf{\Omega}_1), \tag{8}$$

where $\mathcal{B} = \hbar^2/(2Ik_{\mathrm{B}})$ is the rotational constant, $P_J(x)$ is a Legendre polynomial, $\mathbf{\Omega}_2\cdot\mathbf{\Omega}_1 \equiv \cos(\theta_{12})$ is the cosine of the angle between the directions $\mathbf{\Omega}_1$ and $\mathbf{\Omega}_2$, and the primed sum indicates the sum over the *available* angular momentum states of the rotor, to be discussed fully below. For later convenience, we have emphasized the dependence of $f()$ and $\varphi()$ on Λ^2/P and TP, respectively. Note that, with the definitions above, we have

$$q_{\mathrm{rot}}(T,\mathcal{B}) = \int \langle \mathbf{\Omega}|\mathrm{e}^{-\beta K}|\mathbf{\Omega}\rangle \,\mathrm{d}\mathbf{\Omega} = {\sum_{J=0}^{\infty}}' (2J+1)\mathrm{e}^{-\beta\mathcal{B}J(J+1)}. \tag{9}$$

Boltzmann contribution to $B(T)$

The Boltzmann part of $B(T)$ consists in neglecting the contribution from the exchange operator $\mathcal{E}$ in Eq. (5), that is

$$B_{\mathrm{Boltz}}(T) = -\frac{1}{2V}\frac{\Lambda^6}{q_{\mathrm{rot}}^2(T,\mathcal{B})}\int\left(\langle \mathbf{r}_1\mathbf{\Omega}_1;\mathbf{r}_1'\mathbf{\Omega}_1'|\mathrm{e}^{-\beta H}|\mathbf{r}_1\mathbf{\Omega}_1;\mathbf{r}_1'\mathbf{\Omega}_1'\rangle - 1\right)\mathrm{d}^3\mathbf{r}_1\mathrm{d}^3\mathbf{r}_1'\mathrm{d}\mathbf{\Omega}_1\mathrm{d}\mathbf{\Omega}_1', \tag{10}$$

which can be evaluated by using Eq. (6) and inserting $P-1$ completeness relations in the form

$$\mathbf{1} = \int \mathrm{d}^3\mathbf{r}_k \mathrm{d}^3\mathbf{r}'_k \mathrm{d}\boldsymbol{\Omega}_k \mathrm{d}\boldsymbol{\Omega}'_k \; |\mathbf{r}_k\boldsymbol{\Omega}_k;\mathbf{r}'_k\boldsymbol{\Omega}'_k\rangle\langle\mathbf{r}_k\boldsymbol{\Omega}_k;\mathbf{r}'_k\boldsymbol{\Omega}'_k|. \tag{11}$$

After some lengthy but straightforward calculations, Eq. (10) can be written as

$$B_{\mathrm{Boltz}}(T) = -\frac{\Lambda^3}{2}\int \langle\!\langle \exp\left(-\beta\overline{U_2}(\mathbf{R})\right) - 1 \rangle\!\rangle \; \mathrm{d}^3\mathbf{R}, \tag{12}$$

with

$$\overline{U_2}(\mathbf{R}) = \frac{1}{P}\sum_{k=1}^{P} U_2(\mathbf{R}+\mathbf{r}_k-\mathbf{r}'_k;\boldsymbol{\Omega}_k,\boldsymbol{\Omega}'_k). \tag{13}$$

In Eq. (12), the double brackets indicate an average over translational and rotational free-particle paths of the two molecules. The coordinates $\mathbf{r}_k$ and $\boldsymbol{\Omega}_k$ describe the center-of mass position and the orientation of the first molecule, respectively, while the coordinates $\mathbf{r}'_k$ and $\boldsymbol{\Omega}'_k$ describe the second molecule. The double-bracket average implies that the center-of-mass coordinates are sampled from the free-particle probability distribution [21]

$$F(\mathbf{r}_1,\ldots,\mathbf{r}_P) = \Lambda^3\left(\frac{P}{\Lambda^2}\right)^{3P/2}\exp\left[-\frac{\pi P}{\Lambda^2}\sum_{k=1}^{P}|\mathbf{r}_{k+1}-\mathbf{r}_k|^2\right], \tag{14}$$

with the understanding that $\mathbf{r}_{P+1} = \mathbf{r}_1$ and both are equal to the zero vector. Analogously, the orientations are sampled according to

$$\Phi(\boldsymbol{\Omega}_1,\ldots,\boldsymbol{\Omega}_P) = \frac{1}{q_{\mathrm{rot}}}\prod_{k=1}^{P}\varphi(\boldsymbol{\Omega}_{k+1}\cdot\boldsymbol{\Omega}_k), \tag{15}$$

which describes free linear-rotor paths in the space of the possible orientations. [20] Note that also for rotational coordinates one might have $\boldsymbol{\Omega}_{P+1} = \boldsymbol{\Omega}_1$, with $\boldsymbol{\Omega}_1$ uniformly oriented on the sphere. However, as we will discuss in more detail below, in the case of homonuclear diatomics paths can also close on the direction opposite to the initial point (antipode), and hence one must also consider the condition $\boldsymbol{\Omega}_{P+1} = -\boldsymbol{\Omega}_1$. In this case, the two kinds of path

are to be sampled with equal probabilities.

Exchange contribution to $B(T)$

The path-integral evaluation of the exchange contribution of Eq. (5) proceeds similarly to the Boltzmann case, that is by inserting completeness relations of the form (11). However, one has to take into account the fact that the exchange operator $\mathcal{E}$ acts as $\mathcal{E}|\mathbf{r}_1\boldsymbol{\Omega}_1;\mathbf{r}'_1\boldsymbol{\Omega}'_1\rangle = |\mathbf{r}'_1\boldsymbol{\Omega}'_1;\mathbf{r}_1\boldsymbol{\Omega}_1\rangle$. This implies that the end of the path of one molecule closes onto the beginning of the path of the other molecule. Equivalently, one can define $\mathbf{r}'_i = \mathbf{r}_{i+P}$ and $\boldsymbol{\Omega}'_i = \boldsymbol{\Omega}_{i+P}$, resulting in a single path discretized with $2P$ steps, where the first P steps refer to molecule 1 and the last P steps to molecule 2. The expression for the exchange contribution to $B(T)$ then becomes

$$B_{\mathrm{xc}}(T) = -\frac{1}{2V}\frac{\Lambda^6}{q^2_{\mathrm{rot}}(T,\mathcal{B})}\frac{(-1)^S}{n}\int\prod_{i=1}^{2P} f(\mathbf{r}_{i+1},\mathbf{r}_i;\Lambda^2/P)\varphi(\boldsymbol{\Omega}_{i+1},\boldsymbol{\Omega}_i;TP)\exp\left(-\beta\hat{U}_2\right)\,\mathrm{d}^3\mathbf{r}_i\mathrm{d}\boldsymbol{\Omega}_i, \tag{16}$$

where we have defined

$$\hat{U}_2 = \frac{1}{P}\sum_{k=1}^{P} U_2\left(|\mathbf{r}_{k+P}-\mathbf{r}_k|;\boldsymbol{\Omega}_{k+P},\boldsymbol{\Omega}_k\right). \tag{17}$$

As in the Boltzmann case, we have defined $\mathbf{r}_{2P+1} = \mathbf{r}_1$, while the rotational coordinates can either close to the initial bead ($\boldsymbol{\Omega}_{2P+1} = \boldsymbol{\Omega}_1$) or to the antipodal point of the first bead ($\boldsymbol{\Omega}_{2P+1} = -\boldsymbol{\Omega}_1$), as discussed below.

Equation (16) is not yet in the form of an average over translational and rotational paths distributed according to Eqs. (14) and (15). However, we notice that the translational propagator (7) is a function of $\Lambda^2/P = (\sqrt{2}\Lambda)^2/(2P) \equiv \Lambda^2_\mu/(2P)$, enabling us to write $f(\mathbf{r}_{i+1},\mathbf{r}_i;\Lambda^2/P) = f(\mathbf{r}_{i+1},\mathbf{r}_i;\Lambda^2_\mu/(2P))$. Analogously, the rotational propagator (8) is a function of $TP = (T/2)(2P)$ and hence $\varphi(\boldsymbol{\Omega}_{i+1},\boldsymbol{\Omega}_i;TP) = \varphi(\boldsymbol{\Omega}_{i+1},\boldsymbol{\Omega}_i;(T/2)(2P))$. One can then define the distribution probabilities for the translational and rotational coordinates of the

whole path of length $2P$ as

$$F_{\rm xc}(\mathbf{r}_1,\ldots,\mathbf{r}_{2P}) = \Lambda_\mu^3 \prod_{k=1}^{2P} f(\mathbf{r}_{i+1},\mathbf{r}_i;\Lambda_\mu^2/(2P)) \tag{18}$$

$$\Phi_{\rm xc}(\mathbf{\Omega}_1,\ldots,\mathbf{\Omega}_{2P}) = \frac{1}{q_{\rm rot}(T/2,\mathcal{B})} \prod_{k=1}^{2P} \varphi(\mathbf{\Omega}_{k+1}\cdot\mathbf{\Omega}_k;(T/2)(2P)), \tag{19}$$

obtaining

$$B_{\rm xc}(T) = -\frac{\Lambda_\mu^3}{16}\left(\frac{(-1)^S}{n}\right)\frac{q_{\rm rot}(T/2,\mathcal{B})}{q_{\rm rot}^2(T,\mathcal{B})}\left\langle\!\!\left\langle \exp\left(-\beta\hat{U}_2\right)\right\rangle\!\!\right\rangle, \tag{20}$$

where in this case the double angular brackets denote averaging over the translational and rotational coordinates according to the distributions (18) and (19). Note that in the case of point particles $q_{\rm rot}(T,\mathcal{B}) = 1$ and Eq. (20) reduces to the expression derived for atoms.[17]

Sampling single-molecule configurations

In the case of heteronuclear molecules, such as HD, there is no restriction on the available angular moment, and the primed sum in Eq. (8) runs over all nonnegative values of J. For homonuclear molecules, e.g. H_2, one has to take into account the behavior upon exchange of the two nuclei. The nucleus of H is a fermion with nuclear spin $s = \frac{1}{2}$, hence the molecular wavefunction must be antisymmetric upon exchange of the two hydrogen atoms (that is, under the action of the operator $\mathcal{E}$). This means that in the case of an antisymmetric total nuclear spin state ($S = 0 \Rightarrow n = 2S+1 = 1$, p-H_2) only the even values of J (corresponding to states that are even under exchange of the nuclei) contribute to the sum in Eq. (8). Conversely, in the case of a symmetric total nuclear spin state ($S = 1 \Rightarrow n = 3$, o-H_2) only the odd values of J contribute to Eq. (8). The nucleus of D has spin $s = 1$ and is a boson, hence the opposite situation is found: even angular momenta are coupled with even total nuclear spin states ($S = 0, 2 \Rightarrow n = 6$, o-D_2) while odd angular momenta are coupled with odd nuclear spin states ($S = 1 \Rightarrow n = 3$, p-D_2).

The qualitative shape of the rotational propagator of Eq. (8) for various angular momen-

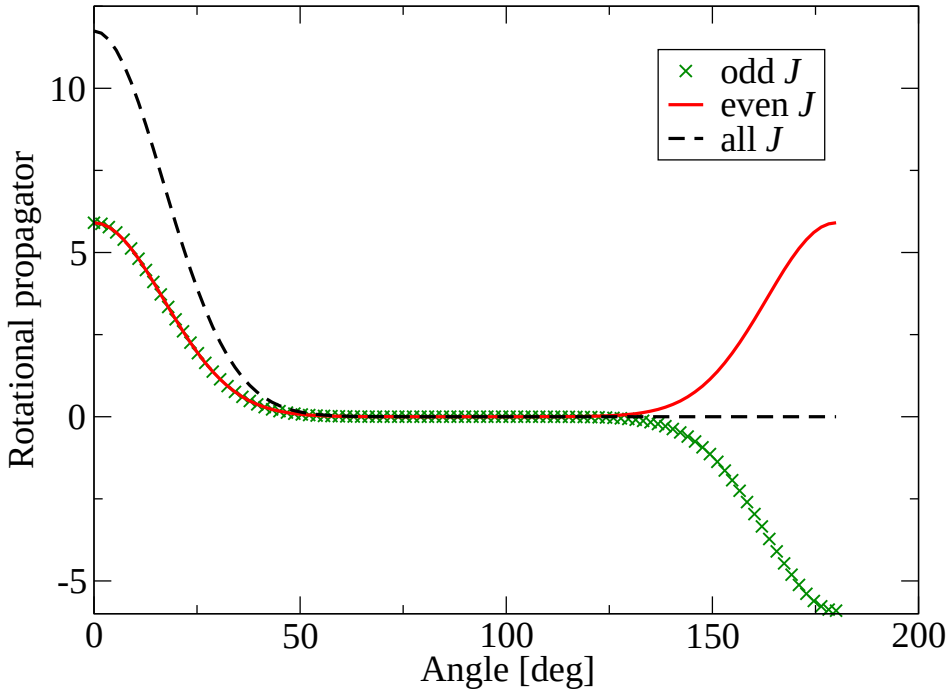

Figure 1: Example values of Eq. (8) for heteronuclear molecules (dashed black line), homonuclear molecules restricted to even angular momentum states (thick red line) and homonuclear molecules restricted to odd angular momentum states (green crosses).

tum states is reported in Fig. 1. The shape of the function for small values of θ_{12} approaches, in the limit $P \to \infty$, a Gaussian function $\varphi \tilde{\propto} \exp\left(-\theta_{12}^2/(2\sigma^2)\right)$ with $\sigma^2 = 2\mathcal{B}/(k_{\mathrm{B}}TP)$.[22]

In the case of homonuclear molecules, the density matrix has two "lobes" around $\theta = 0$ and $\theta = \pi$, as shown in Fig. 1. For even-J molecules the lobes have the same (positive) sign, whereas for odd-J molecules the lobes have opposite signs. This property can be written as $\langle\boldsymbol{\Omega}|\mathrm{e}^{-\beta K_i}|\boldsymbol{\Omega}\rangle = \pm\langle\boldsymbol{\Omega}|\mathrm{e}^{-\beta K_i}|-\boldsymbol{\Omega}\rangle$, where the plus sign is for molecules with even angular momentum states (e.g., p-H_2), and the minus sign for molecules with odd angular momentum states (e.g., o-H_2). As a consequence, one can write, for homonuclear diatomics,

$$q_{\mathrm{rot}}(T,\mathcal{B}) = \int \langle\boldsymbol{\Omega}|\mathrm{e}^{-\beta K_i}|\boldsymbol{\Omega}\rangle \, \mathrm{d}\boldsymbol{\Omega} = \int \frac{\langle\boldsymbol{\Omega}|\mathrm{e}^{-\beta K_i}|\boldsymbol{\Omega}\rangle \pm \langle\boldsymbol{\Omega}|\mathrm{e}^{-\beta K_i}|-\boldsymbol{\Omega}\rangle}{2} \, \mathrm{d}\boldsymbol{\Omega}, \tag{21}$$

which shows that, in the path-integral representations, the (continuous) paths corresponding to the directional coordinate $\mathbf{\Omega}$ are divided into two classes that are to be sampled with equal probability. In the first class, the paths close on the initial direction, while in the second class the paths close on the direction antipodal to the initial one. For even-J molecules (e.g., p-H_2 or o-D_2), the paths connecting one direction to its antipode appear with a positive weight. In the case of odd-J molecules (e.g., o-H_2 or p-D_2), the paths connecting a direction with its antipode are weighted by a negative sign.

Spin isomers with negative weights (o-H_2, p-D_2): the restricted-path approach

In the case of odd angular momenta, the transition "probability" of Eq. (8) has negative regions and direct Metropolis sampling becomes inefficient. However, in this case the contribution from the paths connecting opposite points on the sphere (that is, $\mathbf{\Omega}_{P+1} = -\mathbf{\Omega}_1$, which have a negative weight) are exactly canceled by the paths (with positive weight) that begin and end on the same point on the sphere ($\mathbf{\Omega}_{P+1} = \mathbf{\Omega}_1$), but that extend beyond the hemisphere centered on $\mathbf{\Omega}_1$, which is defined by all the directions $\mathbf{\Omega}$ such that $\mathbf{\Omega}\cdot\mathbf{\Omega}_1 \geq 0$.[23,24] In this case, one only has to sample the paths that begin and end at the same point, while *always* remaining in the same hemisphere; all of these paths have positive weights and pose no difficulty in Monte Carlo sampling.

For the paths restricted to one hemisphere, the equator acts as a repulsive hard barrier. In this case, Barker showed that sampling can be made more efficient by subtracting from the propagator the contribution from images beyond the hard wall.[25] In this case, instead of the "bare" propagator $p(\mathbf{\Omega}_{k+1}|\mathbf{\Omega}_k)$, we use the modified propagator

$$\overline{\varphi}(\mathbf{\Omega}_{k+1}\cdot\mathbf{\Omega}_k) = \varphi(\mathbf{\Omega}_{k+1}\cdot\mathbf{\Omega}_k) - \varphi(\mathbf{\Omega}'_{k+1}\cdot\mathbf{\Omega}_k), \tag{22}$$

where $\mathbf{\Omega}'_{k+1}$ denotes the direction $\mathbf{\Omega}_{k+1}$ reflected through the equator. We note that one can

also use the symmetric form

$$\tilde{\varphi}(\mathbf{\Omega}_{k+1}\cdot\mathbf{\Omega}_k) = \varphi(\mathbf{\Omega}_{k+1}\cdot\mathbf{\Omega}_k) - \frac{1}{2}\left[\varphi(\mathbf{\Omega}'_{k+1}\cdot\mathbf{\Omega}_k)+\varphi(\mathbf{\Omega}_{k+1}\cdot\mathbf{\Omega}'_k).\right], \tag{23}$$

but we could not find any improvement with this choice and therefore used (22) for odd-J rotors. Note that in the case of free rotors as considered here, this restricted-path approach is *exact.*[24]

Sampling paths using Doob's h-transform

The sampling of translational coordinates according to Eq. (14) can be performed very efficiently. From the mathematical point of view, Eq. (14) is the probability distribution for a (discretized) Brownian stochastic process constrained to return to its initial position (the condition $\mathbf{r}_1 = \mathbf{r}_{P+1}$). This stochastic process is also known as a Brownian bridge,[26,27] and it can be sampled very efficiently: several approaches have been developed to sample entire paths[18,28] or for resampling pieces thereof in order to generate new configurations for the acceptance-rejection Metropolis sampling.[29]

To the best of our knowledge, the only approach that has been used to sample free-rotor paths is acceptance-rejection Metropolis sampling, which is the procedure used in our previous works dealing with rigid rotors.[5,30] In this approach, one performs a trial move by displacing one of the coordinates $\mathbf{\Omega}_k$ (chosen randomly) by a random amount, accepting or rejecting the move using the Metropolis method with the probability distribution of Eq. (15). Alternatively, one can perform collective moves using hybrid Monte Carlo techniques.[31] However, these approaches tend to produce highly correlated configurations, and in our past work we took great care to perform a sufficient number of Monte Carlo steps in order to get uncorrelated samples to perform the averages in Eq. (12).

In this paper, we propose a new sampling method for rotational degrees of freedom based

on Doob's h-transform[32,33] that directly produces uncorrelated paths and, additionally, can be used for staging moves when simulating condensed phases involving linear rotors. Doob's h-transform is a powerful technique in the theory of stochastic processes, particularly useful when one needs to modify the behavior of a Markov process to incorporate conditioning or constraints. At its core, the h-transform constructs a new Markov process from an existing one by reweighting its transition probabilities using a positive function h, constrained to preserve certain structural properties of the original process. By suitably choosing the function h, Doob's method enables reshaping the probability measure so that the desired constraint becomes typical in the transformed process.

We give here a heuristic derivation of the h-transform method. Let us consider a Markov stochastic process X_t with transition probability $\pi(y,s|x,t)$ $(s > t)$. Let us assume that $X_0 = x_0$ is the (sharp) initial condition. We want to find the transition probability $\overline{\pi}(y,s|x,t)$ for the process constrained to reach a position x_f at time $\tau > s$, that is with the constraint $X_\tau = x_\mathrm{f}$.

Considering the joint probability $P(A,B,C)$ of events $A : X_t = x$, $B : X_s = y$ and $C : X_\tau = x_\mathrm{f}$, one can write

$$P(A,B,C) = P(C|B,A)P(B|A)P(A), \tag{24}$$

where $P(B|A) = \pi(y,s|x,t)$ and $P(C|B,A) = P(C|B) \equiv h(y,\tau - s)$ is the probability of reaching x_f at τ starting from y at time s. Notice that we have used the Markov property to simplify $P(C|B,A) = P(C|B)$. However, we can also factorize the joint probability as

$$P(A,B,C) = P(B|A,C)P(C|A)P(A), \tag{25}$$

where in this case $P(C|A) = h(x,\tau - t)$ and $P(B|A,C)$ is the transition probability of going from x at time t to y at time s *conditioned* on the requirement of reaching x_f at τ. This latter quantity is the transition probability that we need, hence $P(B|A,C) = \overline{\pi}(y,s|x,t)$. Equating

(24) and (25), we obtain

$$\overline{\pi}(y,s|x,t) = \frac{h(y,\tau-s)}{h(x,\tau-t)}\pi(y,s|x,t), \tag{26}$$

which expresses Doob's h-transform. We still have to find a suitable form for the function $h(x,t)$ that enforces the constraint. Heuristically, one would expect $h(x,\tau-t) = \pi(x_\mathrm{f},\tau|x,t)$, and indeed it can be shown that this is the correct choice, satisfying all the required constraints on h. In particular, this approach recovers the transition probability for Brownian bridges, widely used in performing path-integral Monte Carlo simulations involving only translational coordinates.[26–28] Therefore, we will use the following transition probability in order to sample paths constrained to reach position x_f at (imaginary) time τ:

$$\overline{\pi}(y,s|x,t) = \frac{\pi(x_\mathrm{f},\tau|y,s)}{\pi(x_\mathrm{f},\tau|x,t)}\pi(y,s|x,t). \tag{27}$$

When discretizing the imaginary time with P steps for rotational coordinates, we have that

$$\pi(\mathbf{\Omega}_s,s|\mathbf{\Omega}_t,t) = \varphi\left(\mathbf{\Omega}_s\cdot\mathbf{\Omega}_t;\frac{TP}{s-t}\right), \tag{28}$$

where s and t are integers between 0 and P with $s > t$. In the case of odd-J rotors, the free-particle propagator π is given by Eq. (22), while for even-J and heteronuclear rotors we use Eq. (8).

In order to sample the conditioned propagator of Eq. (27), we use a reweighting method. Starting from point $\mathbf{\Omega}_k$, we sample $N = 200$ positions $\mathbf{\Omega}_{k+1}^{(n)}$ using $\pi(\mathbf{\Omega}_{k+1},k{+}1|\mathbf{\Omega}_k,k)$, compute the weights

$$w_n = \frac{\pi(\mathbf{\Omega}_\mathrm{f},P|\mathbf{\Omega}_{k+1}^{(n)},k+1)}{\pi(\mathbf{\Omega}_\mathrm{f},P|\mathbf{\Omega}_k,k)}, \tag{29}$$

where $\mathbf{\Omega}_\mathrm{f}$ is the final point of the path, and choose the new configuration by sampling with

a probability

$$p_n = \frac{w_n}{\sum_{n=1}^{N} w_n}. \tag{30}$$

The generation of the trial configurations $\Omega_{k+1}^{(n)}$ can be performed straightforwardly by noting that $\varphi(\mathbf{\Omega}_{k+1} \cdot \mathbf{\Omega}_k; TP)$ is a probability distribution that depends only on $\xi = \mathbf{\Omega}_{k+1} \cdot \mathbf{\Omega}_k = \cos\theta_{k,k+1}$, so that one can use inverse transform sampling. After producing a random unit vector $\boldsymbol{\omega}_n$ orthogonal to $\mathbf{\Omega}_k$, one has

$$\mathbf{\Omega}_{k+1}^{(n)} = \xi_n \mathbf{\Omega}_k + \sqrt{1-\xi_n^2}\boldsymbol{\omega}_n. \tag{31}$$

We tested this new sampling method by using it to compute the average rotational kinetic energy $K(T)$ of rigid rotors, evaluated using the standard thermodynamic estimator, and comparing it to the quantum statistical expression

$$K(T) = \mathcal{B}\, \frac{{\sum_{J=0}^{\infty}}' J(J+1)(2J+1)\mathrm{e}^{-\beta\mathcal{B}J(J+1)}}{{\sum_{J=0}^{\infty}}'(2J+1)\mathrm{e}^{-\beta\mathcal{B}J(J+1)}}. \tag{32}$$

The results are shown in Fig. 2 for both p-H_2 and o-H_2, as well as for a fictitious "distinguishable" H_2 molecule (so that the sum in Eq. (8) is on all the angular momentum states J). Doob's h-transform sampling reproduces very well the expected kinetic energy in a large range of temperatures.

Results and discussion

Numerical calculations

We used the two-body hydrogen potential developed in Ref. 13 to compute the second virial coefficient of H_2 and D_2. We set the bondlengths of the various molecules to the ground-state ($J = 0$ or 1) average, computed by numerically solving the Schrödinger equation of a pair of

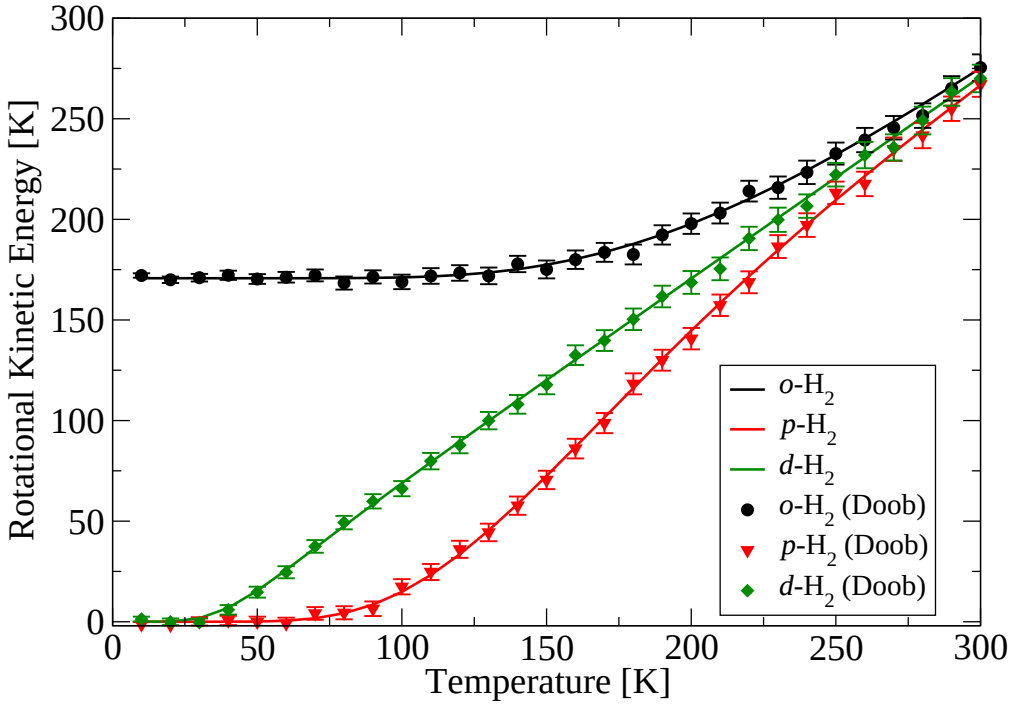

Figure 2: Kinetic energy of H_2 spin isomers. Lines: expected results from Eq. (32). Symbols: results from path-integral simulations using the transition probability of Eq. (27). The label d-H_2 denotes a fictitious "distinguishable" hydrogen molecule where all angular momenta are allowed. Error bars represent expanded ($k = 2$) uncertainties from the path-integral Monte Carlo calculation.

hydrogen atom isotopes interacting via the potential developed by Pachucki.[34] From these calculations, we also evaluated the inertia moment as $1/I = (1/m_r)\langle r^{-2}\rangle$, where m_r is the reduced mass of the pair. The values used in this work are reported in Table 1.

The contribution to the uncertainty in $B(T)$ from the uncertainty in the pair potential was estimated using a generalization to rigid rotors of the functional derivative method developed in Refs. 35 and 36, that is

$$\Delta U_2 = \frac{\Lambda^3}{2} \int \langle\!\langle \beta \overline{\delta U_2}(\mathbf{R}) \mathrm{e}^{-\beta \overline{U_2}(\mathbf{R})} \rangle\!\rangle \, \mathrm{d}^3\mathbf{R}, \tag{33}$$

Table 1: Values of the average bond lengths and inertia moments of hydrogen isotopologues as a function of the angular momentum J, computed using the potential of Ref. 34. Although the average bond length increases with temperature, it shows a significant deviation from its ground-state value only for $T > 100$ K, i.e., at temperatures higher than those considered in this study.[13]

J	H_2 bond length (Å)	H_2 inertia moment (u Å^2)	D_2 bond length (Å)	D_2 inertia moment (u Å^2)
0	0.767155	0.284742	0.759598	0.564554
1	0.768289	0.285602	0.760161	0.565402

where, indicating by δU_2 the uncertainty assigned to the potential, we have defined

$$\overline{\delta U_2}(\mathbf{R}) = \frac{1}{P}\sum_{k=1}^{P} \delta U_2(\mathbf{R} + \mathbf{r}_k - \mathbf{r}'_k; \mathbf{\Omega}_k, \mathbf{\Omega}'_k). \tag{34}$$

We computed $B_{\mathrm{Boltz}}(T)$, $B_{\mathrm{xc}}(T)$, and $\Delta U_2(T)$ using Eqs. (10), (20), and (33), respectively, employing the same temperature-dependent Trotter index P as in our previous work.[5] In the case of the Boltzmann contribution to $B(T)$ and $\Delta U_2(T)$, we used 16 independent free-particle configurations to evaluate the double-bracket average defined in Eq. (12), and we used a modified implementation of the GSL VEGAS routine[37–39] to perform the radial integration, averaging over 5000 independent samples. Statistical uncertainties were evaluated by running 5 independent calculations. In this way, the statistical uncertainty of the calculation turns out to be smaller than the uncertainty propagated from the potential by approximately a factor of five, except at the lowest temperatures investigated. This factor was reduced to ≈ 4 at $T = 3$ K and 4 K, to ≈ 3 at $T = 2$ K, and ≈ 0.5 at $T = 1$ K. The exchange contribution to $B_{\mathrm{xc}}(T)$, Eq. (20), is obtained as a simple average over free-molecule paths, using 32000 independent paths for the computation.

Values of $B(T)$

Values of $B(T)$ for *para*-H_2 computed by the above procedures are presented in Table 2. Importantly, they are consistent with those from our previous study,[13] despite being obtained

using a completely rewritten code and Doob's h-transform sampling of rotational coordinates. This provides independent corroboration and enhances the reproducibility of our findings. Values for *ortho*-H_2 are in Table 3. We limit our calculations to 100 K and below; at higher temperatures higher spin states become dominant and our approximation of using the averaged $J = 0$ and $J = 1$ geometries to represent p-H_2 and o-H_2, respectively, becomes increasingly inaccurate. The temperatures 18.3 K and 20.5 K have been added to our grid of computed points to facilitate comparison with some experimental results.

The Boltzmann and exchange contributions are computed separately. The exchange contribution is relatively small at all temperatures, and negligible above 15 K, so exchange effects cannot account for the measured difference between p-H_2 and n-H_2 near 20 K discussed in the next subsection.

In addition to the "pure" *para* and *ortho* species, we can compute the second virial coefficient of any mixture of spin isomers in the same way $B(T)$ is calculated for a binary mixture:

$$B = x_p^2 B_{pp} + 2x_p x_o B_{po} + x_o^2 B_{oo}, \tag{35}$$

where x is the mole fraction of the spin isomer and the subscripts on B denote the pair of isomers involved in the interaction. The "cross" interaction coefficient B_{po} between *para* and *ortho* species is computed by the methods described above, using the pair potential between one molecule at the $J = 0$ geometry and one at the $J = 1$ geometry; there is no exchange contribution in this case.

This allows us to compute $B(T)$ for n-H_2, for which $x_p = 0.25$ and $x_o = 0.75$. The propagation of uncertainty for n-H_2 requires some care, because the uncertainties from the terms of Eq. (35) are of two types. The statistical uncertainties in the calculated B_{pp}, B_{po}, and B_{oo} are independent and therefore their contributions should be added in quadrature. The uncertainty due to uncertainty in the potential, however, is a systematic effect, and errors from that contribution to B_{pp}, B_{po}, and B_{oo} will be almost 100% correlated. We therefore use the result computed from Eq. (33) for the contribution of uncertainty in the

Table 2: Values of the second virial coefficient $B(T)$ and its components for *p*-H_2. The uncertainty is expanded $k = 2$ uncertainty and includes the propagated uncertainty of the potential and the statistical uncertainty of the path-integral Monte Carlo calculation.

Temperature (K)	Boltzmann (cm^3/mol)	Exchange (cm^3/mol)	Total (cm^3/mol)	Uncertainty (cm^3/mol)
1	−123099	−186	−123285	10600
2	−9706	−59	−9765	349
3	−3443	−28	−3471	93
4	−1870	−16	−1886	40
5	−1231	−10	−1241	22
6	−896	−7	−902	14
7	−698	−5	−702	10
8	−563	−3	−566	8
9	−470	−2.3	−472	6
10	−402	−1.69	−403	5
12	−308	−0.93	−309	4
15	−223	−0.42	−223	3
18.3	−167.4	−0.19	−167.6	1.9
20	−147.6	−0.13	−147.7	1.6
20.5	−142.4	−0.12	−142.5	1.6
25	−106.3	−0.04	−106.4	1.2
30	−80.8	−0.016	−80.8	1.0
35	−63.2		−63.2	0.8
40	−50.5		−50.5	0.7
45	−40.9		−40.9	0.6
50	−33.5		−33.5	0.5
75	−12.1		−12.1	0.3
100	−2.2		−2.2	0.3

Table 3: Values of the second virial coefficient $B(T)$ and its components for *o*-H_2. The uncertainty is expanded $k = 2$ uncertainty and includes the propagated uncertainty of the potential and the statistical uncertainty of the path-integral Monte Carlo calculation.

Temperature (K)	Boltzmann (cm^3/mol)	Exchange (cm^3/mol)	Total (cm^3/mol)	Uncertainty (cm^3/mol)
1	−135960	−21	−135980	9931
2	−10484	−7	−10490	387
3	−3571	−3	−3574	94
4	−1918	−2	−1920	39
5	−1259	−1.1	−1260	22
6	−912	−0.7	−913	14
7	−708	−0.5	−709	11
8	−572	−0.3	−572	8
9	−476	−0.3	−476	6
10	−406	−0.2	−406	5
12	−310	−0.10	−310	4
15	−225	−0.05	−225	3
18.3	−169.0	−0.02	−169.0	1.9
20	−148.7	−0.014	−148.7	1.7
20.5	−143.4	−0.013	−143.4	1.6
25	−107.2	−0.005	−107.2	1.2
30	−81.4		−81.4	1.0
35	−63.7		−63.7	0.8
40	−50.9		−50.9	0.7
45	−41.3		−41.3	0.6
50	−33.7		−33.7	0.5
75	−12.2		−12.2	0.3
100	−2.3		−2.3	0.3

potential at any composition. Finally, the statistical uncertainty and potential uncertainty contributions are added in quadrature to yield the combined uncertainty for n-H_2 or any mixture composition.

The results for the *para*/*ortho* cross interaction in H_2, along with those for n-H_2, are given in Table 4.

Comparison with experimental $B(T)$ data for p-H_2 for the potential used here may be found in Ref. 13. As shown in Ref. 14, the effect of flexibility in the calculation of $B(T)$ is significant compared to the uncertainties of the experimental results. For n-H_2, our result at 100 K in Table 4 differs by less than 0.5 $cm^3\,mol^{-1}$ from that obtained by interpolating the two lowest-temperature points (98 K and 103 K) reported by Michels et al.[40] At lower temperatures, there are only a few scattered, older sources for n-H_2. We defer a more thorough comparison with experimental $B(T)$ to future work that will incorporate the effect of flexibility.

Similar calculations were performed for o-D_2, p-D_2, and n-D_2. Results for o-D_2 are in Table 5, for p-D_2 in Table 6, and for the *para*/*ortho* cross interaction along with n-D_2 in Table 7.

Comparison with experimental spin isomer effect

Almost all experimental studies of $B(T)$ for H_2 measured only one form, either p-H_2 or n-H_2. Because of differences in measurement techniques, different temperatures, inherent uncertainty in individual experiments, etc., these studies are not useful for evaluating the difference due to spin isomers.

We therefore restrict our comparison to the work of Beenakker et al.,[6] who designed a differential apparatus to measure the difference between spin isomers in a single experiment. Because the difference is small (on the order of 1% of the magnitude of $B(T)$ at these temperatures), only a differential measurement could reliably resolve this small difference.

Beenakker et al. reported their results in Amagat units, which were common in that era

Table 4: Values of the second cross virial coefficient between *p*-H_2 and *o*-H_2 ($B_{pH_2-oH_2}$) and for the normal mixture of *p*-H_2 and *o*-H_2 ($B(nH_2)$). The uncertainties are expanded $k = 2$ uncertainties and include the propagated uncertainty of the potential and the statistical uncertainty of the path-integral Monte Carlo calculation.

Temperature (K)	$B_{pH_2-oH_2}$ (cm^3/mol)	$U(B_{pH_2-oH_2})$ (cm^3/mol)	$B(nH_2)$ (cm^3/mol)	$U(B(nH_2))$ (cm^3/mol)
1	−125930	9962	−131418	7656
2	−9987	353	−10256	351
3	−3484	93	−3534	92
4	−1890	39	−1907	39
5	−1236	22	−1250	22
6	−900	15	−908	14
7	−700	10	−705	10
8	−567	8	−570	8
9	−473	6	−475	6
10	−403	5	−405	5
12	−308	4	−310	4
15	−224	3	−224	3
18.3	−168.1	1.9	−168.6	1.6
20	−147.8	1.6	−148.3	1.2
20.5	−142.6	1.6	−143.1	0.9
25	−106.8	1.2	−107.0	0.8
30	−81.0	1.0	−81.3	0.7
35	−63.3	0.8	−63.6	0.8
40	−50.7	0.7	−50.8	0.7
45	−41.1	0.6	−41.2	0.6
50	−33.5	0.5	−33.6	0.5
75	−12.2	0.3	−12.2	0.3
100	−2.2	0.3	−2.3	0.3

Table 5: Values of the second virial coefficient $B(T)$ and its components for *o*-D_2. The uncertainty is expanded $k = 2$ uncertainty and includes the propagated uncertainty of the potential and the statistical uncertainty of the path-integral Monte Carlo calculation.

Temperature (K)	Boltzmann (cm^3/mol)	Exchange (cm^3/mol)	Total (cm^3/mol)	Uncertainty (cm^3/mol)
1	−13035277	−10	−13035287	2349262
2	−84573	−3	−84576	5417
3	−12837	−1.0	−12838	519
4	−4794	−0.5	−4795	142
5	−2540	−0.2	−2540	61
6	−1624	−0.14	−1624	33
7	−1147	−0.08	−1147	21
8	−870	−0.05	−870	14
9	−692	−0.028	−692	11
10	−569	−0.017	−569	8
12	−412		−412	5
15	−283		−283	3
20	−179		−179	2
25	−126.3		−126.3	1.4
30	−94.6		−94.6	1.1
35	−73.4		−73.4	0.9
40	−58.3		−58.3	0.7
45	−47.3		−47.3	0.6
50	−38.7		−38.7	0.6
75	−14.8		−14.8	0.4
100	−3.8		−3.8	0.3

Table 6: Values of the second virial coefficient $B(T)$ and its components for *p*-D_2. The uncertainty is expanded $k = 2$ uncertainty and includes the propagated uncertainty of the potential and the statistical uncertainty of the path-integral Monte Carlo calculation.

Temperature (K)	Boltzmann (cm^3/mol)	Exchange (cm^3/mol)	Total (cm^3/mol)	Uncertainty (cm^3/mol)
1	−17987215	−6	−17987222	2711698
2	−94367	−1.7	−94369	5246
3	−13919	−0.7	−13920	517
4	−4997	−0.3	−4997	148
5	−2617	−0.2	−2617	60
6	−1653	−0.1	−1653	33
7	−1164	0.0	−1165	21
8	−886	0.0	−886	14
9	−700	−0.018	−700	11
10	−576	−0.011	−576	8
12	−417		−417	5
15	−286		−286	3
20	−181		−181	2
25	−127.0		−127.0	1.4
30	−95.2		−95.2	1.1
35	−73.8		−73.8	0.9
40	−58.7		−58.7	0.7
45	−47.6		−47.6	0.6
50	−38.9		−38.9	0.6
75	−14.8		−14.8	0.4
100	−3.9		−3.9	0.3

Table 7: Values of the second cross virial coefficient between *o*-D_2 and *p*-D_2 ($B_{oD_2-pD_2}$) and for the normal mixture of *o*-D_2 and *p*-D_2 ($B(nD_2)$). The uncertainties are expanded $k = 2$ uncertainties and include the propagated uncertainty of the potential and the statistical uncertainty of the path-integral Monte Carlo calculation.

Temperature (K)	$B_{oD_2-pD_2}$ (cm^3/mol)	$U(B_{oD_2-pD_2})$ (cm^3/mol)	$B(nD_2)$ (cm^3/mol)	$U(B(nD_2))$ (cm^3/mol)
1	−17485667	3447905	−15563448	1769504
2	−85479	5711	−86066	4980
3	−13114	533	−13081	504
4	−4837	145	−4836	139
5	−2563	62	−2559	60
6	−1628	34	−1629	33
7	−1150	21	−1150	20
8	−876	15	−874	14
9	−694	11	−694	10
10	−570	8	−570	8
12	−413	6	−413	5
15	−285	3	−284	3
20	−180	2	−180	2
25	−126.6	1.4	−126.5	1.4
30	−94.9	1.1	−94.8	1.1
35	−73.5	0.9	−73.5	0.9
40	−58.5	0.7	−58.4	0.7
45	−47.4	0.6	−47.4	0.6
50	−38.9	0.6	−38.8	0.6
75	−14.8	0.4	−14.8	0.4
100	−3.8	0.3	−3.8	0.3

but are now obscure. An amagat is the density or specific volume of a gas at a standard temperature of 0 °C and standard pressure of 1 atm (0.101 325 MPa). Because gases differ slightly in their deviation from ideal-gas behavior, an amagat of hydrogen is not quite the same as an amagat of another gas. For hydrogen, we used the equation of state of Leachman et al.[41] for n-H_2 to compute the amagat volume of 22 428 $cm^3\,mol^{-1}$. In principle, an amagat of p-H_2 would be slightly different, but that difference is negligible in our context.

Beenakker et al. performed three measurements of $B_{p\text{-}H_2} - B_{n\text{-}H_2}$ at 20.5 K. The average of their three results was 1.81 $cm^3\,mol^{-1}$, and they claimed an accuracy of 5%. At 18.3 K, the average difference was 2.13 $cm^3\,mol^{-1}$, but the claimed accuracy was only 20%. They attempted a similar measurement on D_2, but found that $B_{o\text{-}D_2} - B_{n\text{-}D_2}$ was too small to measure within the sensitivity of their apparatus. This was largely due to the lower vapor pressure of D_2 that reduced the range of measurement, but also due to the fact that the difference in composition between the low-temperature form of D_2 (*ortho*) and the normal form (2/3 *ortho*) is smaller than for H_2.

We can compute the difference $B_{p\text{-}H_2} - B_{n\text{-}H_2}$ in a straightforward manner from the results in Tables 2 and 4. The uncertainty of this difference, however, is smaller than a simple combination of the uncertainty columns in those two tables would produce. First, since any error due to the potential will be nearly identical for the different states, the part of the combined uncertainty due to uncertainty in the potential must be removed; only the statistical uncertainty is relevant. Second, the statistical uncertainty in the n-H_2 calculation contains a component from p-H_2 that cancels when taking a difference. The expanded uncertainty in the difference is related to the statistical uncertainties in the individual calculations (U_{pp}, U_{po}, and U_{oo}) by

$$U_{\text{diff}}^2 = \left[(1 - x_p^2)U_{pp}\right]^2 + \left[2x_p x_o U_{po}\right]^2 + \left[x_o^2 U_{oo}\right]^2 , \tag{36}$$

with $x_p = 0.25$ and $x_o = 0.75$.

In Fig. 3, we compare our calculated differences $B_{p\text{-}H_2} - B_{n\text{-}H_2}$ to those reported by Beenakker et al.[6] Our results clearly show an effect in the correct direction, but the magni-

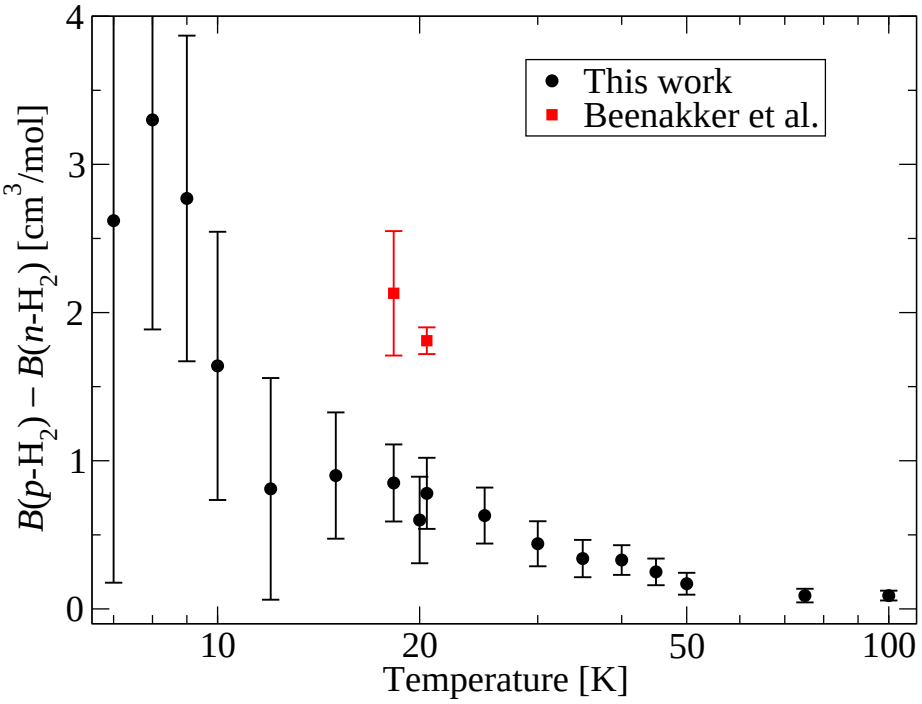

Figure 3: Calculated $B_{p\text{-}H_2} - B_{n\text{-}H_2}$ compared to experimental results of Beenakker et al.[6] Error bars for calculations represent expanded ($k = 2$) uncertainties; for Beenakker et al. they are the authors' reported "accuracy."

tude seems to be smaller than that from experiment by roughly a factor of two.

We similarly calculated the difference between the low-temperature and high-temperature forms of D_2, $B_{o\text{-}D_2} - B_{n\text{-}D_2}$, based on the calculations reported in Tables 5 and 7. We found it to be (0.33 ± 0.09) cm^3/mol at $T = 20$ K, roughly a factor of 3 smaller than the difference calculated for H_2. This is consistent with the report of Beenakker et al.[6] that, unlike the case of H_2, this difference for D_2 at 20.5 K was too small to be determined within the precision of their experiments.

Conclusions

We have developed an approach to apply path-integral methods to calculating virial coefficients for rigid rotors that accounts for the complication of *para* and *ortho* spin states. Unlike previous work that was restricted to even values of the spin quantum number (e.g., p-H_2), we can compute $B(T)$ for o-H_2, n-H_2, etc. The combination of Doob's h-transform (which guarantees that sampled paths are uncorrelated) and restricted-path sampling with a modified propagator enables efficient computation of what would otherwise be a challenging sampling problem for species with odd rotational states. Moreover, the use of Doob's h-transform to sample constrained paths with a known transition probability has potential applications beyond the present context. An immediate example is path-integral sampling of non-linear rigid rotors, such as water.[42,43]

When comparing our results with the only available experimental data, shown in Fig. 3, we see that our calculations yield a difference $B_{p\text{-}H_2} - B_{n\text{-}H_2}$ that has the correct sign and is of the right order of magnitude. However, the computed difference is approximately a factor of two smaller than the experimental value. We can identify three possible reasons for this discrepancy.

First, the problem could lie with the experiments, which represent a single study 65 years ago. While the group reporting the result was well-regarded, they were measuring a small differential effect, and an error cannot be ruled out. Independent measurement of this quantity with modern techniques would be welcome.

Second, there could be an issue with the pair potential. While the rigid part of the potential we used has small and well-defined uncertainties,[5] the additional contribution for flexibility[12] was developed primarily for bound dimer states and its uncertainty, especially for the repulsive states that also contribute to $B(T)$, is not clear.

Finally, our treatment of the molecules as rigid rotors could have affected the difference. It was shown in Ref. 14 that fully incorporating flexibility into the calculation of $B(T)$ had a non-negligible effect compared to a rigid-rotor calculation. While one might expect the

effect of fully incorporating flexibility to be similar for the odd and even spin states, perhaps there is some reason why that effect varies between $J = 0$ and $J = 1$. We intend to extend the framework developed here for odd rotational states to use a flexible H_2 potential, which will test this possibility.

After this work was completed, we were made aware of a new six-dimensional pair potential[44] that should be more accurate than that developed in Ref. 13. Calculations with this new potential can be used both to test the second possibility above (possible deficiencies of the pair potential used) and the third (effect of flexibility).

Acknowledgement

The authors are grateful to J. Karl Johnson for facilitating what has turned into a long and fruitful collaboration, the spark for which was one of us seeing a presentation of the work of Ref. 10. We also thank Joe Magee of NIST for encouragement to explore the effect of spin isomers on hydrogen properties, and a reviewer for making us aware of Ref. 44.

References

(1) Al Ghafri, S. Z. S.; Munro, S.; Cardella, U.; Funke, T.; Notardonato, W.; Trusler, J. P. M.; Leachman, J.; Span, R.; Kamiya, S.; Pearce, G. et al. Hydrogen liquefaction: a review of the fundamental physics, engineering practice and future opportunities. *Energy Environ. Sci.* **2022**, *15*, 2690–2731.

(2) Siłkowski, M.; Pachucki, K.; Komasa, J.; Puchalski, M. Leading-order QED effects in the ground electronic state of molecular hydrogen. *Phys. Rev. A* **2023**, *107*, 032807.

(3) Rychlewski, J. An accurate calculation of the polarizability of the hydrogen molecule and its dependence on rotation, vibration and isotopic substitution. *Mol. Phys.* **1980**, *41*, 833–842.

(4) Sun, D.; Zhang, Y. P.; Wei, X. J.; Wang, L. M.; Yan, Z.-C. Polarizabilities of hydrogen molecules calculated without using the Born-Oppenheimer approximation. *Phys. Rev. A* **2021**, *103*, 062813.

(5) Patkowski, K.; Cencek, W.; Jankowski, P.; Szalewicz, K.; Mehl, J. B.; Garberoglio, G.; Harvey, A. H. Potential energy surface for interactions between two hydrogen molecules. *J. Chem. Phys.* **2008**, *129*, 094304.

(6) Beenakker, J. J. M.; Varekamp, F. H.; Knaap, H. F. P. The second virial coefficient of ortho and para hydrogen at liquid hydrogen temperatures. *Physica* **1960**, *26*, 43–51.

(7) Cohen, E. G. D.; Offerhaus, M. J.; van Leeuwen, J. M. J.; Roos, B. W.; De Boer, J. The transport properties and the equation of state of gaseous para- and ortho-hydrogen and their mixtures below 40°K. *Physica* **1956**, *22*, 791–815.

(8) Boyd, M. E.; Larsen, S. Y. Quantum Mechanical Calculations of the Second Virial Coefficients for Hydrogen. National Bureau of Standards Technical Note 412., 1967; Available at: `https://doi.org/10.6028/NBS.TN.412`.

(9) Knaap, H. F. P.; Beenakker, J. J. M. The Lennard-Jones 6–12 potential parameters of H_2 and D_2. *Physica* **1961**, *27*, 523–530.

(10) Diep, P.; Johnson, J. K. An accurate H_2–H_2 interaction potential from first principles. *J. Chem. Phys.* **2000**, *112*, 4465–4473, Erratum, *113*, 3480 (2000).

(11) Harvey, A. H.; Hodges, M. P. The effect of anisotropy on the second virial coefficient of H_2. *J. Chem. Phys.* **2000**, *113*, 3474–3476.

(12) Hinde, R. J. A six-dimensional H_2–H_2 potential energy surface for bound state spectroscopy. *J. Chem. Phys.* **2008**, *128*, 154308.

(13) Garberoglio, G.; Jankowski, P.; Szalewicz, K.; Harvey, A. H. Second virial coefficients of H_2 and its isotopologues from a six-dimensional potential. *J. Chem. Phys.* **2012**, *137*, 154308.

(14) Garberoglio, G.; Jankowski, P.; Szalewicz, K.; Harvey, A. H. Path-integral calculation of the second virial coefficient including intramolecular flexibility effects. *J. Chem. Phys.* **2014**, *141*, 044119.

(15) Hirschfelder, J. O.; Curtiss, C. F.; Bird, R. B. *Molecular Theory of Gases and Liquids*; John Wiley & Sons: New York, 1954.

(16) Hill, T. L. *Statistical Mechanics*; Dover: New York, 1987.

(17) Garberoglio, G.; Harvey, A. H. Path-integral calculation of the third virial coefficient of quantum gases at low temperatures. *J. Chem. Phys.* **2011**, *134*, 134106, Erratum: *152*, 199903 (2020).

(18) Fosdick, L. D.; Jordan, H. F. Path-integral calculation of the two-particle Slater sum for He^4. *Phys. Rev.* **1966**, *143*, 58–66.

(19) Feynman, R. P.; Hibbs, A. *Quantum Mechanics and Path Integrals*; McGraw-Hill: New York, 1965.

(20) Marx, D.; Müser, M. H. Path integral simulations of rotors: theory and applications. *J. Phys. Cond. Mat.* **1999**, *11*, R117–R155.

(21) Garberoglio, G. Boltzmann bias grand canonical Monte Carlo. *J. Chem. Phys.* **2008**, *128*, 134109.

(22) Müser, M. H. The Path-Integral Monte Carlo of Rigid Linear Molecules in Three Dimensions. *Mol. Sim.* **1996**, *17*, 131–141.

(23) Pollock, E.; Runge, K. J. Two low temperature applications of path integrals: superfluidity in ^{4}He and orientational ordering in solid H_2, D_2. *Physica B* **1994**, *197*, 180–188.

(24) Ceperley, D. M. In *Molecular Dynamics of Condensed Matter Systems*; Binder, K., Ciccotti, G., Eds.; Editrice Compositori: Bologna, Italy, 1996.

(25) Barker, J. A. A quantum-statistical Monte Carlo method; path integrals with boundary conditions. *J. Chem. Phys.* **1979**, *70*, 2914–2918.

(26) Karatzas, I.; Shreve, S. *Brownian Motion and Stochastic Calculus*; Graduate Texts in Mathematics; Springer-Verlag: New York, 1991; Vol. 113.

(27) Chow, W. C. Brownian bridge. *WIREs Comput. Stat.* **2009**, *1*, 325–332.

(28) Levy, P. *Memorial des Sciences Mathematiques*; Gauthier Villars: Paris, 1954; Fascicule 126.

(29) Ceperley, D. M. Path integrals in the theory of condensed helium. *Rev. Mod. Phys.* **1995**, *67*, 279–355.

(30) Garberoglio, G. On the three-body contributions to the third virial coefficient of parahydrogen. *Chem. Phys. Lett.* **2013**, *557*, 26–30.

(31) Garberoglio, G.; Johnson, J. K. Hydrogen Isotope Separation in Carbon Nanotubes: Calculation of Coupled Rotational and Translational States at High Densities. *ACS Nano* **2010**, *4*, 1703–1715, arXiv:cond-mat/0703287.

(32) Doob, J. L. Conditional Brownian motion and the boundary limits of harmonic functions. *Bull. Soc. Math. France* **1957**, *85*, 431–458.

(33) Doob, J. L. *Classical potential theory and its probabilistic counterpart*; Classics in Mathematics; Springer-Verlag: New York, 1984; Vol. 262.

(34) Pachucki, K. Born–Oppenheimer potential for H_2. *Phys. Rev. A* **2010**, *82*, 032509.

(35) Garberoglio, G.; Harvey, A. H. Path-integral calculation of the fourth virial coefficient of helium isotopes. *J. Chem. Phys.* **2021**, *154*, 104107.

(36) Garberoglio, G.; Gaiser, C.; Gavioso, R. M.; Harvey, A. H.; Hellmann, R.; Jeziorski, B.; Meier, K.; Moldover, M. R.; Pitre, L.; Szalewicz, K. et al. *Ab Initio* Calculation of Fluid Properties for Precision Metrology. *J. Phys. Chem. Ref. Data* **2023**, *52*, 031502.

(37) Lepage, G. P. A new algorithm for adaptive multidimensional integration. *J. Comput. Phys.* **1978**, *27*, 192–203.

(38) Galassi, M.; Davies, J.; Theiler, J.; Gough, B.; Jungman, G.; Alken, P.; Booth, M.; Rossi, F. *GNU Scientific Library: Reference Manual*, 3rd ed.; Network Theory Limited, 2009.

(39) Garberoglio, G. parallel_vegas. GitHub repository, `https://github.com/gioGarbe/parallel_vegas`, 2025; Accessed: 2024-09-01.

(40) Michels, A.; de Graaff, W.; Ten Seldam, C. A. Virial coefficients of hydrogen and deuterium at temperatures between −175°C and +150°C. Conclusions from the second virial coefficient with regards to the intermolecular potential. *Physica* **1960**, *26*, 393–408.

(41) Leachman, J. W.; Jacobsen, R. T.; Penoncello, S. G.; Lemmon, E. W. Fundamental Equations of State for Parahydrogen, Normal Hydrogen, and Orthohydrogen. *J. Phys. Chem. Ref. Data* **2009**, *38*, 721–748.

(42) Noya, E. G.; Sesé, L. M.; Ramírez, R.; McBride, C.; Conde, M. M.; Vega, C. Path integral Monte Carlo simulations for rigid rotors and their application to water. *Mol. Phys.* **2011**, *109*, 149–168.

(43) Noya, E. G.; Vega, C.; McBride, C. A quantum propagator for path-integral simulations of rigid molecules. *J. Chem. Phys.* **2011**, *134*, 054117.

(44) Jóźwiak, H.; Stolarczyk, N.; Stankiewicz, K.; Zaborowski, M.; Lisak, D.; Wójtewicz, S.; Jankowski, P.; Patkowski, K.; Szalewicz, K.; Thibault, F. et al. Accurate reference spectra of HD in an H_2–He bath for planetary applications. *Astron. & Astrophys.* **2024**, *687*, A69.
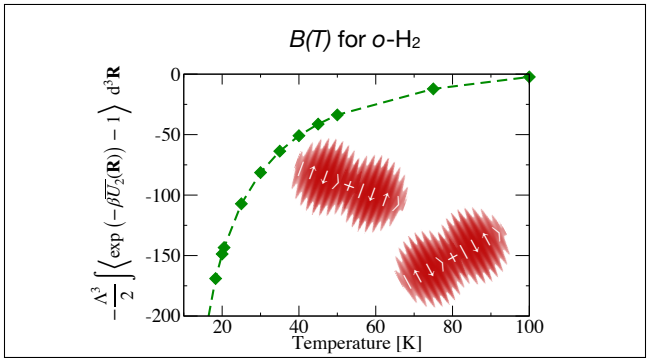
TOC Graphic